Spin dynamics of Mn$_{12}$-acetate in the thermally activated tunneling regime: ac susceptibility and magnetization relaxation

Teemu Pohjola[1,2] and Herbert Schoeller[3]

[1]*Materials Physics Laboratory, Helsinki University of Technology, 02015 HUT, Finland*
[2]*Institut für Theoretische Festkörperphysik, Universität Karlsruhe, 76128 Karlsruhe, Germany*
[3]*Forschungszentrum Karlsruhe, Institut für Nanotechnologie, Karlsruhe, Germany*

In this work, we study the spin dynamics of Mn$_{12}$-acetate molecules in the regime of thermally assisted tunneling. In particular, we describe the system in the presence of a strong transverse magnetic field. Similar to recent experiments, the relaxation time/rate is found to display a series of resonances; their Lorentzian shape is found to stem from the tunneling. The dynamic susceptibility $\chi(\omega)$ is calculated starting from the microscopic Hamiltonian and the resonant structure manifests itself also in $\chi(\omega)$. Similar to recent results reported on another molecular magnet, Fe$_8$, we find oscillations of the relaxation rate as a function of the transverse magnetic field when the field is directed along a hard axis of the molecules. This phenomenon is attributed to the interference of the geometrical or Berry phase. We propose susceptibility experiments to be carried out for strong transverse magnetic fields to study these oscillations and for a better resolution of the sharp satellite peaks in the relaxation rates.

I. INTRODUCTION

In recent years, numerous experimental results on macroscopic samples of molecular magnets, especially Mn$_{12}$-acetate and Fe$_8$-triazacyclononane, have drawn attention to the peculiar resonant structure observed in the hysteresis loops and relaxation time measurements,[1–4] as well as in the dynamic susceptibility.[2,5] In this paper, we concentrate on Mn$_{12}$ (shorthand for Mn$_{12}$-acetate). At low temperature, the observed relaxation times τ are long, up to several months and more, and display a series of resonances with faster relaxation as a function of an external magnetic field directed along the easy (z) axis of the sample. These are considered as signs of macroscopic quantum tunneling (MQT) of magnetization.

Typical experimental samples consist of single crystals or ensembles of aligned crystallites of identical Mn$_{12}$ molecules. Each molecule has eight Mn^{3+} and four Mn^{4+} ions which, in their ferromagnetic ground state, have a total spin $S=10$. Due to strong anisotropy along one of the crystalline axes (z direction), there is a high potential barrier

$$U(S_z) = -AS_z^2 - BS_z^4, \quad (1)$$

with $A/k_B \approx 0.54$ K and $B/k_B \approx 0.0011$ K, between the opposite orientations of the spin ($S_z = \pm 10$); the easy axis is the same for all the molecules.[6] The dipolar interaction between the molecular spins, a possible relaxation mechanism, has been found to be weak in Mn$_{12}$.[7,8] Instead, the observed resonant phenomena are attributed to quantum *tunneling* of single spins—the response being magnified by the large number of them—interacting with the phonons in the lattice. The role of the hyperfine interactions is still under some controversy and is only briefly touched upon in the following.

The main features of the experimental findings can be understood in terms of two competing relaxation mechanisms: quantum-mechanical tunneling *through* and thermal activation *over* the anisotropy barrier. At high temperatures ($T>3$ K or $T>6$ K, depending on the experiment[9]), the spins relax predominantly via thermal activation due to the phonons in the lattice.[10–12] In this regime, the relaxation time follows the Arrhenius law $\tau = \tau_0 \exp(U/k_B T)$, where $U/k_B \approx 60$ K denotes the barrier height and $\tau_0 \approx 10^{-8}$ s the inverse attempt frequency.[13] When temperature is lowered to $2<T<3$ K, the time required by the over-barrier relaxation increases exponentially but several of the excited states still remain thermally populated. An external magnetic field can be used to bring pairs of states on the opposite sides of the barrier to degeneracy enhancing the probability to tunnel across the barrier. The tunneling arises due to crystalline anisotropy and possible transverse magnetic field at the site of the spin. The tunneling amplitudes are the larger the closer to the top of the barrier the states are and, consequently, the thermal population of the higher states plays a key role in relaxation, cf., e.g. Refs. 10–12 and 14. At still lower temperatures, tunneling and the relaxation becomes sensitive to fluctuations in the dipolar and hyperfine fields.[15] In this paper, we concentrate in the regime of thermally activated tunneling.

Several authors have investigated the spin dynamics theoretically with the emphasis ranging from "minimal" models, assuming as simple a spin Hamiltonian $\mathcal{H}_S$ and a model of the surroundings as possible (in order to explain experiments, that is),[10–12,14,16–18] to more specific models for investigating the role of the dipolar and/or hyperfine interactions,[19–21] and combinations of these.[12,14,16,22] The thermally activated relaxation has typically been studied using a master equation approach to describe the time evolution of the spin-density matrix.[10–12,14,16–18,23] The susceptibility, on the other hand, has only been treated within a phenomenological model.[5,24–26]

The existing theories have been successful in explaining the general features seen in experiments. However, several

points call for further attention. (i) A microscopic calculation of the dynamic susceptibility is missing altogether. (ii) The effect of a strong transverse magnetic field has not been thoroughly studied and, in particular, not in the context of the susceptibility.[25] (iii) Several authors including ourselves have found a series of side resonances to arise in their calculations[16,18,23]—the fact that these peaks are not in general (see Ref. 27 for exceptions) observed in experiments is not quite clear. In this work, we aim at elucidating these points and present calculations for the relaxation rates and susceptibility in a unified language that can be conveniently extended to systems with stronger couplings. We work with a Hamiltonian similar to, e.g., Ref. 18, cf. Eqs. (2)–(4), but introduce an alternative framework to work with the density matrix. It is well known that all the resonances can be enhanced by a strong transverse magnetic field but we show that the resonances can also be reduced and even suppressed: Both the relaxation rate, see also Ref. 22, and susceptibility are found to display significant dependence on the direction of the transverse field suggesting that interference effects of a geometrical phase could be observed also in Mn$_{12}$ and, what is more, do so in the regime of thermally activated tunneling.

The paper is organized as follows. Section II introduces the microscopic model used for Mn$_{12}$ and a discussion on the different interaction mechanisms in the system. In Sec. III, we develop a time-dependent description of the system in terms of a kinetic equation and the resulting master equation governing the spin dynamics. The kinetic equation is solved for the field-dependent relaxation times $\tau(H)$ and the static susceptibility $\chi_0(H)$. The dynamic susceptibility $\chi(\omega;H)$ is calculated in Sec. III B and a Kubo-type formula is found. Section IV displays the numerical results for both $\tau(H)$ and $\chi(\omega;H)$ accompanied with a discussion on the results and their relevance to experiments. In Sec. V we sum up the work.

II. SYSTEM

The spin Hamiltonian of a single Mn$_{12}$ molecule can be written in the form $\mathcal{H}_S = \mathcal{H}_z + \mathcal{H}_T$. The first term,

$$\mathcal{H}_z = -A S_z^2 - B S_z^4 - g \mu_B H_z S_z, \qquad (2)$$

with S_z being the spin component along the easy axis (here the z direction), describes the part that commutes with S_z. It consists of the anisotropy terms of Eq. (1) and a Zeeman term which enables external biasing of the energies. The anisotropy constants have been experimentally estimated[28,29] as $A/k_B = 0.52$–0.56 K and $B/k_B = 0.0011$–0.0013 K; the g factor is 1.9.[30] The resulting energy levels E_m for the eigenstates of $S_z|m\rangle = m|m\rangle$ together with the potential barrier are shown schematically in Fig. 1.

The second term in the Hamiltonian,

$$\mathcal{H}_T = -\frac{1}{2} B_4 (S_+^4 + S_-^4) - g \mu_B (H_x S_x + H_y S_y), \qquad (3)$$

does not commute with S_z and gives rise to tunneling. The B_4 term arises from crystalline anisotropy, $B_4 = (4.3$–$14.4) \times 10^{-5}$ K (below we use $B_4 = 8.6 \times 10^{-5}$ K, but the particular choice is unimportant for the results obtained),[28]
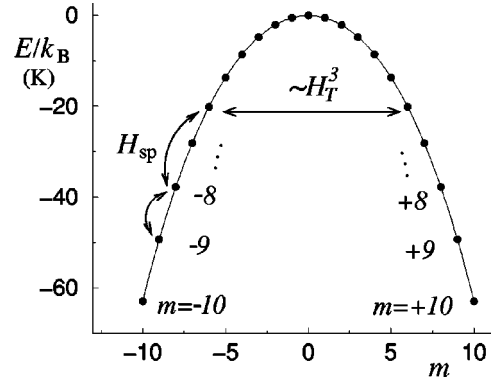

FIG. 1. Schematic of the energy diagram for $2S+1=21$ eigenstates of $\mathcal{H}_z$ together with the functional form of the potential barrier (solid line). The figure also shows examples of possible transition processes: spin-phonon coupling may change m by ± 1 or ± 2, while the anisotropy term in $\mathcal{H}_T$ yields tunnel couplings across the barrier – an example of a third-order (in B_4) process is depicted in the figure.

while the second term is the Zeeman term corresponding to a transverse magnetic field $H_\perp = H \sin \theta$ (in spherical coordinates, θ is the polar angle away from the z axis; the azimuth angle is denoted ϕ: $H_x = H_\perp \cos \phi$ and $H_y = H_\perp \sin \phi$).

Figure 2 shows the eigenenergies of $\mathcal{H}_S$ as a function of the longitudinal magnetic field H_z. Away from the resonances, the eigenstates $|d\rangle$ resemble the states $|m\rangle$ and are also localized onto the different sides of the barrier—the linear field dependence of the eigenenergies stems from the Zeeman term in Eq. (2). Close to the resonances, $\mathcal{H}_T$ couples the $|m\rangle$ states across the barrier and gives rise to avoided crossings in the energy diagram for E_d. The magnitude of these splittings directly gives the tunneling strengths. Depending on the states in question as well as on the magnitude of B_4 ($H_\perp = 0$ for the moment), the splittings are found to vary enormously: from 10^{-10} K for the choice $B_4/k_B = 4.3 \times 10^{-5}$ K and the states $m = \pm 10$ up to almost 2 K for $B_4/k_B = 14.4 \times 10^{-5}$ K and the resonance $m = \pm 2$. This upper limit is already of the same order of magnitude as the
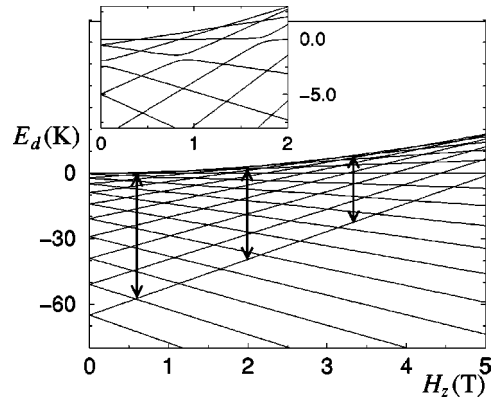

FIG. 2. The eigenenergies of the 21 states as a function of H_z. The inset shows a blow up of the higher energies at low fields—note especially the avoided crossings of the states $m-m' = 4$ directly coupled by the B_4 term in $\mathcal{H}_T$. There are similar, although smaller, splittings for the lower levels as well. The three arrows denote the effective barrier height that decreases with increasing H_z.
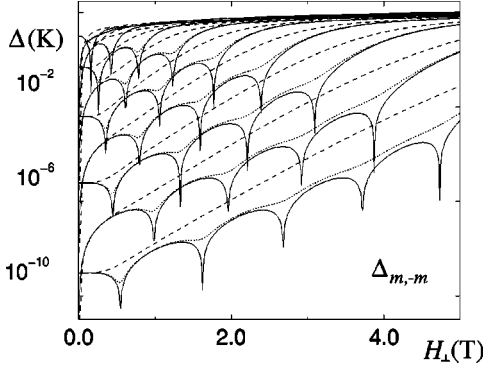
FIG. 3. The tunnel splittings $\Delta_{m,-m}$ as a function of the transverse magnetic field; $H_z = 0$. The three types of curves correspond to three different angles ϕ: $0°$, dashed; $40°$, dotted; and $45°$, solid.

level spacing and in fact even exceeds it rendering perturbative calculations of the tunneling couplings/strengths somewhat questionable. Therefore, even though we first formulate everything in a general form, independent of the choice of basis for the spins, we calculate the actual results working in the eigenbasis of $\mathcal{H}_S$. This choice of basis provides the additional advantage that it allows us to consider arbitrarily strong magnetic fields.

In absence of $H_\perp$, there is a selection rule to $\mathcal{H}_T$: only states m and m' that are a multiple of four apart are coupled. Experimental data do not lend support to such a rule, however, but rather suggest that all transitions are allowed. It turns out that already a tiny transverse field in Eq. (3) is sufficient in achieving this—such a field may arise due to dipolar and/or hyperfine interactions within the sample, see below, as well as due to uncertainty in the precise angle between the external field and the easy axis of the sample. We assume throughout the paper a small constant misalignment angle $\theta = 1°$ and $H_\perp = |\mathbf{H}| \cdot \sin \theta$. In places, we wish to investigate the effects of a significantly stronger transverse field and state so explicitly. The transverse field increases the tunnel splittings if ϕ is close to $n\pi/2$ (n is an integer), i.e., along the x and y axes, or leads to oscillations in the splittings if ϕ is close to one of the directions $\pi(2n+1)/4$. Below we denote these special directions as the hard axes of the molecules.[31] The tunnel splittings are illustrated in Fig. 3 as a function of $H_\perp$ and for different angles ϕ, see Ref. 32.

The usage of $\mathcal{H}_S$ of an isolated spin is based, first of all, on the assumption that the molecules indeed reside in their $S=10$ ground state.[34] This is well justified for the experimental temperatures below 3–6 K—the energy required to excite the system to the lowest excited state with $S=9$ is around 30 K. The second assumption is the absence of interaction. In reality, the spins interact with each other via dipolar interaction, with the nuclear spins via hyperfine interaction, and with the phonons of the surrounding lattice. Experimental evidence shows that the dipolar interactions are small for $T > 2$–2.4 K,[15,35] while the hyperfine interactions produce an intrinsic broadening of the order of 10 mT to the spin states.[12,35] We neglect these for the moment and return to them in Sec. IV C.

The spin-phonon interaction is mediated by variations in the local magnetic field induced by lattice vibrations and distortions. For tetragonal symmetry, this can be generally formulated as, cf. Ref. 18,

$$\mathcal{H}_{sp} = g_1(\epsilon_{xx} - \epsilon_{yy}) \otimes (S_x^2 - S_y^2) + \frac{1}{2} g_2 \epsilon_{xy} \otimes \{S_x, S_y\}$$

$$+ \frac{1}{2} g_3(\epsilon_{xz} \otimes \{S_x, S_z\} + \epsilon_{yz} \otimes \{S_y, S_z\})$$

$$+ \frac{1}{2} g_4(\omega_{xz} \otimes \{S_x, S_z\} + \omega_{yz} \otimes \{S_y, S_z\}), \quad (4)$$

where $\epsilon_{\alpha\beta}$ and $\omega_{\alpha\beta}$ are the symmetric and antisymmetric strain tensors, respectively, and g_i ($i=1,2,3,4$) are the spin-phonon coupling constants. For these, we adopt the values from Ref. 18: $g_1 \approx g_4/2 = A$ and $|g_2| \approx g_1$ and $|g_3| \approx g_4$.[36] In leading order in g_i's, $\mathcal{H}_{sp}$ produces transitions such that, for, $g_{1,2}$ terms, $\Delta m = \pm 2$ and, for $g_{3,4}$ terms, $\Delta m = \pm 1$. The phonons themselves are described by

$$\mathcal{H}_{ph} = \sum_{\vec{k}\sigma} \omega_{\vec{k}\sigma} b_{\vec{k}\sigma}^{\dagger} b_{\vec{k}\sigma} \quad (5)$$

as a bath of noninteracting bosons.

To be more quantitative, the phonons are assumed to be plane waves with a linear spectrum and three modes—two transverse and one longitudinal—denoted by σ. The elements of the strain tensor, $\epsilon_{\alpha\beta} \equiv (\partial_\alpha u_\beta + \partial_\beta u_\alpha)/2$ and $\omega_{\alpha\beta} \equiv (\partial_\alpha u_\beta - \partial_\beta u_\alpha)/2$, are defined in terms of the local displacement vector

$$u_\alpha(\vec{r}) = \sum_{\vec{k}\sigma} \sqrt{\frac{\hbar}{2NM\omega_{\vec{k}\sigma}}} e_\alpha^{(\sigma)}[b_{\vec{k}\sigma}^{\dagger} + b_{\vec{k}\sigma}] e^{i\vec{k}\cdot\vec{r}}. \quad (6)$$

Here $b_{\vec{k}\sigma}^{(\dagger)}$ are the bosonic operators for phonons with wave vector $\vec{k}$, $\omega_{\vec{k}\sigma}$ is the corresponding frequency, and $e_\alpha^{(\sigma)}$ the αth element (of x, y, and z) of the polarization vector; N is the number of unit cells and M the mass per unit cell.

Above we considered the energy scales inherent to $\mathcal{H}_S$, and the spin-phonon rates, which are found below (Appendix A) to be typically of the order of 10^{-5}–10^{-4} K, fall in between the extremes of the tunnel splittings. This value is very small compared to the stronger tunneling couplings and seems to suit well for a perturbative treatment. On the other hand, for the low-lying and weakly coupled states the spin-phonon rates may be several orders of magnitude larger than the tunnel splittings and one would expect the tunneling to be suppressed. However, the intermediate regime, where the tunneling and spin-phonon rates are of the same order of magnitude, requires some extra care; see below.

III. DYNAMICS

The magnetization measured in experiments is the molecular magnetization $M(t) = g\mu_B\langle S_z(t)\rangle$ magnified by the large number of molecules in the samples. In order to calculate this, we start with the general formulation

$$\langle S_z(t)\rangle = \mathrm{Tr}[S_z(t) \cdot \rho_0^{tot}], \quad (7)$$

where $\rho_0^{tot} = \rho^S \rho^{ph}$ denotes the initial density matrix of the whole system encompassing the spin and phonon degrees of freedom. The interaction between the two is assumed to be

turned on adiabatically and only enters the time evolution of $S_z(t)$ (in Heisenberg picture and with the convention $\hbar = 1$)

$$\langle S_z(t) \rangle = \text{Tr}(e^{+i \int_{t_0}^{t} dt' \mathcal{H}(t')} S_z e^{-i \int_{t_0}^{t} dt' \mathcal{H}(t')} \cdot \rho_0^{\text{tot}}). \qquad (8)$$

Expansion of the exponentials and a standard elimination of the phonon degrees of freedom leads to an effective description of the spin in terms of a reduced density matrix $\rho(t) = \text{Tr}_{\text{ph}}[\rho^{\text{tot}}(t)]$. The details of the calculation can be found in Ref. 38, where we also introduce a real-time diagrammatic formalism[40] for expressing and evaluating all the quantities to follow. The reduced density matrix $\rho(t)$ describes the full time evolution of the spin degrees of freedom in the presence of the spin-phonon interaction and, e.g., the magnetization takes the form

$$M(t) = g \mu_B \langle S_z(t) \rangle \equiv g \mu_B \text{Tr}_S[S_z \rho(t)] = g \mu_B \sum_m m \cdot \rho_{m,m}(t). \qquad (9)$$

The diagonal elements $\rho_{m,m}(t)$ are just the probabilities for the spin to be in the states $|m\rangle$.

A. Kinetic equation

The time evolution of $\rho(t)$ is governed by the kinetic equation

$$\dot{\rho}(t) + i[\mathcal{H}_S, \rho(t)] = \int_0^t dt' \Sigma(t,t') \rho(t'). \qquad (10)$$

The commutator on the left-hand side of Eq. (10) corresponds to the free (Hamiltonian) time evolution of the spin, while the integral on the right-hand side describes a dissipative interaction which is nonlocal in time and contains the spin-phonon coupling terms. The kernel $\Sigma(t,t') = \Sigma(t-t')$ is derived in Ref. 38 and the expressions needed for its evaluation are given in Appendix A up to order $O(g^2)$. It depends only on the time difference since the Hamiltonian is time-translationally invariant. According to Eq. (A8), we find that $\Sigma(t-t')$ is a fast decaying function of time, and we make the simplifying Markov assumption that $\rho(t)$ remains essentially constant over the time period Δt within which $\Sigma(t-t')$ decays to zero and take $\rho(t)$ in front of the integral.[41] This is justified at least for the longest relaxation time τ_1 (see below). For convenience, we also take the upper integration limit to infinity.

After taking $\rho(t)$ out of the integral in Eq. (10) the integration over time (up to infinity) can be performed and we are left with a constant Σ. Equation (10) becomes

$$\dot{\rho}(t) = -i L_0 \rho(t) + \Sigma \rho(t) \equiv W \rho(t) \qquad (11)$$

with $L_0 \equiv [\mathcal{H}_S, .]$. This is similar to the master equation formulations in the literature[12,14,16–18] and may be solved for the eigensolutions of W:

$$\dot{\rho}^{(i)}(t) = W \rho^{(i)}(t) = \lambda_i \rho^{(i)}(t) \qquad (12)$$

$$\rho^{(i)}(t) = \rho^{(i)}(0) \cdot e^{\lambda_i t}. \qquad (13)$$

The real parts of the eigenvalues correspond to relaxation rates $\text{Re}(\lambda_i) = -\tau_i^{-1}$.

The eigensolution of W with $\lambda_0 = 0$ corresponds to the stationary state, defined as $\dot{\rho}^{(0)}(t) = 0$ with $\rho^{(0)}(t) = \rho^{(0)}$. The diagonal elements of are the thermal probabilities to find the spin in the respective states. In the m basis, the static magnetization and susceptibility are readily expressed in terms of the diagonal components $\rho_m^{(0)} = \rho_{m,m}^{(0)}$ yielding

$$M_0 = g \mu_B \sum_m m \rho_m^{(0)}, \qquad (14)$$

$$\chi_0 = \frac{\partial M_0}{\partial H_z} = g \mu_B \sum_m m \cdot \frac{\partial \rho_m^{(0)}}{\partial H_z}. \qquad (15)$$

Since the stationary probabilities are given by Boltzmann factors we obtain in the absence of tunneling

$$\chi_0 = -\frac{(g \mu_B)^2}{k_B T} \sum_{m,m'} m(m'-m) \rho_m^{(0)} \rho_{m'}^{(0)}. \qquad (16)$$

In the presence of tunneling, this form remains essentially the same up to transverse fields of the order of 1 T (in this range most of the tunneling splittings are too small compared to the level spacing in order to change the result considerably).

For all the other solutions $\text{Re}(\lambda_i) < 0$ and the vectors $\rho^{(i)}(t)$ correspond to deviations from $\rho^{(0)}$. The longest relaxation time τ_1 is several orders of magnitude larger than τ_2 and the respective solution is interpreted to correspond to the interwell relaxation, i.e., from one side of the barrier onto the other.

Above we have considered the full (reduced) density matrix $\rho(t)$. In Appendix B, we discuss the choice of the basis and argue that the d basis has certain advantages and, e.g., in the case of strong tunneling compared to the spin-phonon rates, it allows the restriction to the diagonal elements of $\rho(t)_{d,d'}$ only. The nondiagonal elements become important when the rates for the tunneling and the spin-phonon coupling are of the same order of magnitude.

B. ac susceptibility

In this section we outline the derivation of the dynamic susceptibility

$$\chi(\omega) \equiv \int_0^\infty d\tau e^{i\omega\tau} \chi(\tau), \qquad (17)$$

$$\chi(t-t') = \frac{\partial M(t)}{\partial H_z(t')} = g \mu_B \frac{\partial \langle S_z(t) \rangle}{\partial H_z(t')}. \qquad (18)$$

For convenience, we assume in the following that $H_\perp$ can be tuned to any (static) value independent of H_z and that the actual measurement is done by applying a tiny ac-excitation field $h_z(\omega)$ on top of the static H_z. The more general calculation of $\partial M_\alpha(t)/\partial H_\beta(t')$, $\alpha, \beta = x, y, z$, can be carried out along the same lines.

In Ref. 38 we show that the derivation with respect to $H_z(t')$ yields

$$\chi(t-t') = i(g\mu_B)^2 \langle [S_z(t), S_z(t')] \rangle \quad (19)$$

which, when inserted to Eq. (17), is just the Kubo formula for the linear response to an external magnetic field. The diagrammatic evaluation of Eq. (19) leads to the expression

$$\chi(\omega) = -(g\mu_B)^2 \sum_{d,d',d''} m_d \left[\frac{1}{-i\omega + iL_0 - \Sigma(\omega)} \right]_{d,d''}$$

$$\times \tilde{\Sigma}(\omega)_{d'',d'} \rho_{d'}^{(0)}, \quad (20)$$

where $\Sigma(\omega)$ is defined as the Laplace transform of $\Sigma(t,0)$, and $\tilde{\Sigma}(\omega)$ is an auxiliary function arising from the derivative of $\Sigma(t,0)$ with respect to $H_z(t')$. The explicit expressions for $\tilde{\Sigma}(\omega)_{d,d''}$ turn out lengthy and are omitted here.

The resolvent in Eq. (20) is treated in terms of the eigensolutions of $W\rho(t)$ and the appropriate projections of the terms $\tilde{\Sigma}(\omega)\rho^{(0)} = \Sigma_i c_i \rho^{(i)}$ are used. In particular, for the component along the relaxing mode $\rho^{(1)}(t)$, the resolvent in Eq. (20) reads

$$\frac{1}{-i\omega + iL_0 - \Sigma(\omega)} = \frac{1}{-i\omega - W(\omega)} \approx \frac{1}{-i\omega + \tau_1^{-1}}.$$

The approximate sign is due to the Markov approximation where $\Sigma(\omega) \approx \Sigma(0)$, cf. Appendix C. Apart from one τ_1 this is the well-known factor in expressions for susceptibility, see, e.g., Refs. 44 or 24. The rest of Eq. (20) reduces to a prefactor roughly proportional to τ_1^{-1} but with weak H_z and ω dependences. The respective projections along the other modes turn out to be proportional to the time constants τ_i. These are very small and render all these terms negligible for the frequencies considered below. Therefore we are left with the effective formula for the susceptibility

$$\chi(\mathbf{H},T,\omega) \approx \frac{\chi_0(\mathbf{H},T)}{1 - i\omega\tau_1(\mathbf{H},T)}, \quad (21)$$

which has been widely used in explaining experiments, see, e.g., Ref. 5. For the low-frequency limit, we recover the static susceptibility, i.e., $\lim_{\omega \to 0} \chi(\omega) = \chi_0$ where χ_0 is given by Eq. (16).

IV. RESULTS

In this section, we concentrate on results obtained in the eigenbasis of $\mathcal{H}_S$. This choice is advocated by three points. First, it allows us to consider much stronger transverse fields (see the discussion on energy scales in Sec. II) than the common approach to calculate tunnel splittings in the leading-order perturbation theory;[39,14] second, the origin of the Lorentzian shape of the resonances is seen to arise naturally from the tunnel splittings.[16,23] The third point is that, in this basis, all the relevant properties of the system are captured by the diagonal elements $\rho(t)_{d,d}$ only.[43] This feature also improves the performance of the numerics. We also present results obtained with the full $\rho(t)$ and discuss the differences as examples of phonon-induced decoherence. The energies are expressed in kelvin, magnetic fields in teslas, and rates in s^{-1}.
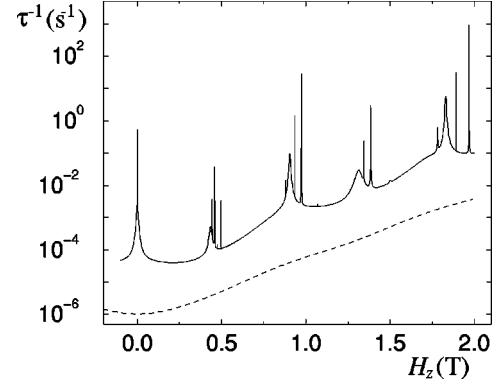

FIG. 4. Relaxation rate $\Gamma = 1/\tau$ as a function of the longitudinal magnetic field: without tunneling (dashed) and with tunneling (solid). Here, only the diagonal density matrix elements are used. The large offset between the two curves is due to the broad Lorentzian shapes under the even resonances: there is a strong direct coupling between the states $m = -m' = -2$ around $H_z = 0$, $m = -3, m' = 1$ under the second series of peaks ($H_z \approx 2H_1$), and $m = -4, m' = 0$ under the fourth series of peaks ($H_z \approx 4H_1$). The sharp resonances arise due to tunnel coupling of lower-lying states m; their height reflects the energies E_m via the Arrhenius law $\Gamma \propto \exp[-\beta(E_m - E_{-10})]$, and the peak width is given by the tunnel splitting. Here the temperature is 2.5 K.

A. Relaxation rates

The relaxation rate as a function of the longitudinal magnetic field H_z is shown in Fig. 4. The overall behavior is of the Arrhenius form, i.e., $\tau \approx \tau_0 \exp[\beta U(H_z)]$ where τ_0 only gives a constant offset to the semilogarithmic figure and U is the effective height of the barrier; see Fig. 2. On top of this exponential field dependence, there are series of resonances located at

$$H_z^{m,m'} = -\frac{m+m'}{g\mu_B}[A + B(m^2 + m'^2)] \quad (22)$$

corresponding to the values of the external field that brings the states m and m' on resonance; the resonances form groups close to the fields $H_z \approx nH_1$ where $n = m + m'$ and $H_1 = A/g\mu_B$, see Fig. 4. The broadest of the resonances resemble those seen in usual experiments, while most of the resonances are too narrow to be seen and, as is discussed below, already the phonon coupling is sufficient to suppress them. One of the main topics of this paper is the possibility to detect some of the satellite peaks by the application of a relatively strong transverse field $H_\perp$ as well as to suppress the already visible peaks by pointing $H_\perp$ along one of the hard axes.

The whole curve in Fig. 4 can be understood in terms of the expression

$$\tau^{-1} = \sum_n [\tau_0^{(n)}]^{-1} D_n(H_z) e^{-\beta U_n(H_z)}, \quad (23)$$

where the index n enumerates the resonances (pairs of states m_n and m_n'). As discussed in Appendix D, there is a certain $\tau_0^{(n)}$ for each resonance; the function $D_n(H_z)$ is a tunneling-induced Lorentzian that yields the peak shapes, and $U_n(H_z)$ is the effective barrier height for the nth resonance, i.e., U_n

$=E_{m_n}-E_{-10}$ (E_{-10} is the energy of the metastable minimum). The widths of the Lorentzian peaks are given by

$$\delta H_z = \frac{4|\Delta_n|}{g\mu_B|m_n-m'_n|}, \qquad (24)$$

where $2|\Delta_n|$ is the tunnel splitting between the resonant states, cf. Appendix D. As is seen in the figure and also suggested by the inset in Fig. 2, the background is not given by the over-barrier relaxation but by the "leakage" due to the direct coupling of states with $m-m'=\pm4$, e.g., $m=\pm2,m'=\mp2$ close to $H_z=0$ and $m=\pm1,m'=\mp3$ close to $H_z=2H_1$. This effectively lowers the barrier height to $U\approx E_{-2}-E_{-10}$. The rates that determine $\tau_0^{(n)}$, depend only weakly on temperature, the resonant states, and H_z, cf. Appendix D. This is in line with the experimental observation that the estimated prefactor of the Arrhenius law, τ_0, varies within an order of magnitude for different samples and resonances.

The sharpness of the narrowest peaks in Fig. 4 is an artifact of the reduced model used so far, i.e., neglect of the nondiagonal matrix elements, and let us next consider two things affecting these peaks: decoherence due to spin-phonon coupling and the broadening effect of a transversal magnetic field $H_\perp$. For other contributions such as the hyperfine and dipolar interactions, see Sec. IV C.

The decay of the nondiagonal elements of the density matrix is a classical definition of decoherence and this is also what is seen here when the above calculation is performed using the full $\rho(t)$. Inclusion of the off-diagonal elements still produces Lorentzian peaks but now the narrow resonances—with widths of the same order of magnitude as the spin-phonon coupling—are broadened and reduced in height. The narrowest peaks may even be completely suppressed, see the solid-line curves in Fig. 5. Despite its intuitive appeal, the suppression of the narrow peaks should be taken only qualitatively because of the limitations of the Born approximation used in treating the spin-phonon coupling. For this reason, the following considerations are restricted to regimes where the effect of the nondiagonal elements of $\rho(t)$ is negligible.

The suppressing effect of the spin-phonon coupling being essentially a constant, the sharper resonances can be made observable by broadening them with a transverse field $H_\perp$; even ground-state tunneling has been observed in high enough fields.[46] The various tunnel splittings are shown in Fig. 3 as a function of $H_\perp$ pointed to three different directions ϕ. It can be seen that for small values of the field, the splittings are essentially independent of the chosen angle, see also Fig. 6. Furthermore, tunnel splittings between states that can be coupled with sole B_4 terms of $\mathcal{H}_T$ are quite insensitive to the transverse field below 0.1–0.2 T. Figure 5 illustrates the effect of $H_\perp=H_x$ onto the two first series of peaks. The resonances that initially ($H_x=0$) were broader than $\tau_0^{(n)-1}$ are seen to retain their height; the narrower peaks, such as the two shown in the insets, are strongly broadened with increasing H_x and also their heights increase once their widths become larger than the spin-phonon rates.

A transverse field cannot only increase the tunnel splittings but it can also reduce them, see Fig. 3. In the ideal case,
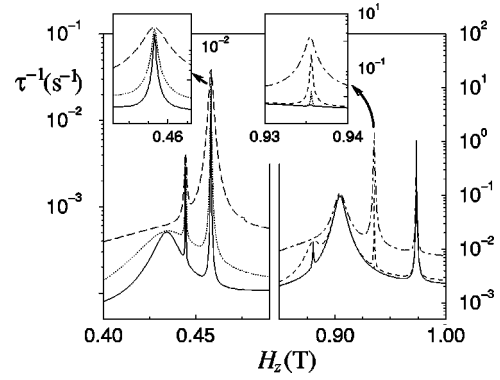

FIG. 5. Magnification of the first and second clusters of peaks of Fig. 4 magnified (solid line). The different curves correspond to: $H_\perp=0.0$ T (solid), 0.01 T (dotted), 0.05 T (dashed), 0.1 T (long dashed), and 0.2 T (dot dashed); $\phi=0°$ for all the curves. The peaks further to the right correspond to resonances between lower states, hence the higher maxima. The peaks (from left to right) correspond to the resonances $m=1,\ldots,4$, $m'=-m-1$ in the left figure (the two first ones are merged together) and $m=2,\ldots,5$, $m'=-m-2$ in the right figure. Here we used also the off-diagonal elements of $\rho(t)$ with the result that some of the sharper peaks are reduced in height or even suppressed due to spin-phonon coupling. The peak widths show strong $H_\perp$ dependence except for the second and fourth peaks on the right—these arise from B_4^2 and B_4^3 type of coupling. Once the peak widths due to the tunnel splittings exceed the phonon-induced width, the peak heights are essentially determined by the energy $U_n=E_n-E_{-10}$ needed to reach the resonant states.

the splittings can even be suppressed by varying the angle ϕ where the transverse field is pointed. For the zeroth peak, i.e., for $H_z\approx0T$, all ten resonances occur at the same position and the suppression of any one of them is obscured in the relaxation rate curves by the simultaneous broadening of other resonances. For this reason, let us first focus on the resonances occurring at finite H_z and return to the $H_z\approx0$ case in the next section.

Figure 6 shows the tunnel splittings $\Delta_{4,-5}$ and $\Delta_{3,-5}$, respectively, as a function of $H_\perp$ and for four different values
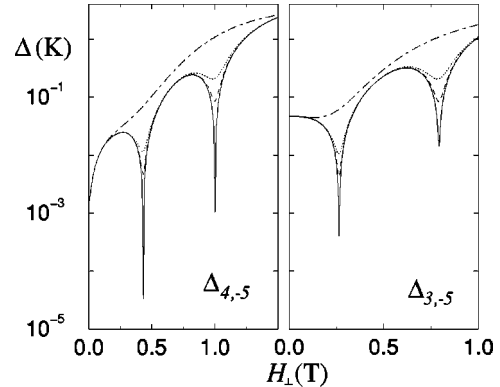

FIG. 6. The tunnel splittings $\Delta_{4,-5}$ (left) and $\Delta_{3,-5}$ (right) as a function of the transverse magnetic field when H_z is kept fixed at the position of the corresponding resonance, 0.4581 T and 0.9045 T, respectively. In both figures, the four curves correspond to different angles ϕ: 0°, dot-dashed; 40°, dotted; 43°, dashed; and 45°, solid; the vertical axes are the same.
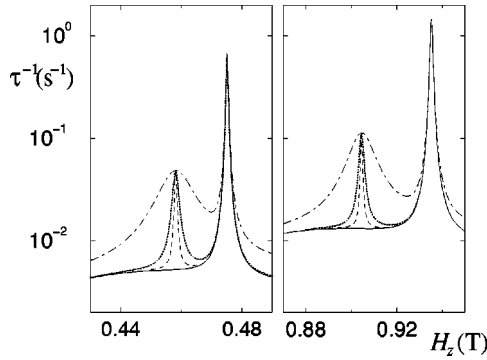
FIG. 7. Relaxation rate τ^{-1} as in Fig. 5 but now for stronger transverse field $H_\perp$ and for different angles ϕ. The line types and angles are as in Fig. 6 and the values of $H_\perp = 0.4311$ T and 0.2643 T are chosen to match the first suppression points (for the actual suppression occurring at the minimum value for Δ the values for $H_\perp$ should be given with even higher accuracy). Temperature is 2.5 K.

of ϕ. The former corresponds to the resonance shown in the left inset of Fig. 5, while the latter corresponds to the broad resonance in the right panel of Fig. 5—this is also the one seen in experiments at $H_z \approx 2H_1$. Figure 6 also exemplifies some general properties of the tunnel splittings. As already mentioned above, the Δ's depend only weakly on ϕ for low $H_\perp$, while for larger fields and ϕ close to the hard axes, the tunneling amplitudes are successively increased and reduced as $H_\perp$ is increased. On the other hand, with $H_\perp$ held fixed to one of the suppression points, the Δ's oscillate as a function of ϕ. Similar to recent work on Fe$_8$, see, e.g., Ref. 47, these phenomena are attributed to alternating constructive and destructive interference of the geometrical phase in the tunneling amplitudes.[48,49] The number of minima for a given $\Delta_{m,m'}$ appears to be, as was also pointed out in Ref. 22, given by the number of B_4 terms involved in coupling the states m and m'. This ranges from zero at the top of the barrier to five for the ground states $m = \pm 10$, cf. Fig. 3.

Figure 7 shows the relaxation rates corresponding to the resonances of Fig. 6 with $H_\perp$'s chosen to match the first points of suppression $H_\perp^{m,m'}$. The resonance width is found to be very sensitive to ϕ quite as expected and, for $\phi = 45°$, the left-most peak becomes suppressed. Note, that the suppression is also quite sensitive to the value of $H_\perp$ as well and the higher peaks in Fig. 7 are hardly affected at all by changes in ϕ.

B. ac susceptibility

This section contains the main results of this paper: study of the interference effects in the dynamic susceptibility $\chi(\omega)$. The results are based on the approximate expression, Eq. (21), obtained above for the susceptibility $\chi(\omega)$, and the results for the relaxation time τ_1 of the previous section. Figure 8 illustrates the two contributions to Eq. (21) (in all figures, the susceptibility is expressed for a single spin and in units of K T^{-2}).

In the present model, the main correction to Eq. (21) corresponds to an intrawell mode describing transitions between the two lowest states on the same side of the anisotropy barrier. This correction increases with increasing H_z and
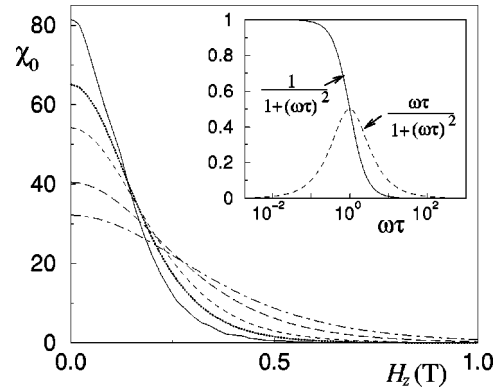

FIG. 8. Static susceptibility χ_0 as a function of the longitudinal magnetic field shown for different temperatures: 2 K (solid), 2.5 K (dotted), 3 K (dashed), 4 K (long dashed), and 5 K (dot dashed). The dynamic susceptibility $\chi(\omega)$ is essentially composed of χ_0 multiplied by the real and imaginary parts of $1/(1 - i\omega\tau)$ shown in the inset as the solid and dashed lines, respectively.

temperature and, for the parameters and the curves of χ_0 in Fig. 8, becomes of the same order of magnitude as the actual relaxing mode once $H_z \approx 0.9$–1 T. However, such a mode corresponds to very high frequencies and is neglected below. There could be also other sources of high-frequency contributions such as dipole-dipole flip flops, nuclear spin dynamics, or moving impurities but these are beyond the scope of this work.

As to the actual results, it is in principle sufficient to combine the curves for τ of the previous section with those shown in Fig. 8. The shapes of the real and imaginary parts of $1/(1 - i\omega\tau)$ readily imply how the resulting susceptibility behaves if one fixes ω—it turns out that all the structure found in τ^{-1} in the previous section can also be found in $\chi(\omega)$. First, the response is the most sensitive to changes in τ when $\omega \approx \tau^{-1}$ or $\omega\tau \approx 1$, cf. the inset of Fig. 8. Second, Re$[\chi(H_z; \omega)]$ replicates the shape of $\tau(H_z)$ and exhibits peaks and valleys as τ^{-1} increases and decreases. This is the case with the imaginary part, Im$[\chi(H_z; \omega)]$, as well, but only as long as $\omega\tau \gtrsim 1$, i.e., as long as we remain on the right
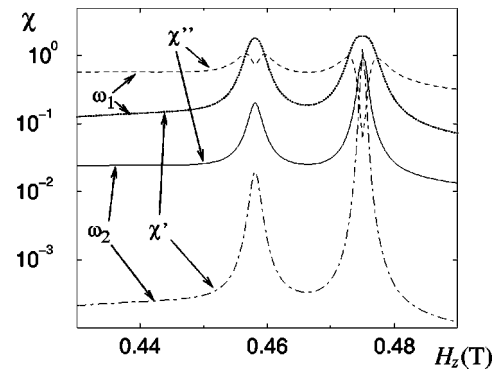

FIG. 9. The real and imaginary parts of susceptibility for the same parameters as the dotted curves in the left panels of Fig. 7, i.e., $H_\perp = 0.4311$ T, $\phi = 40°$, and $k_B T = 2.5$ K. The curves correspond to frequencies $\omega_1 = 0.02$ Hz, χ' (dotted); χ'' (dashed); and $\omega_2 = 0.5$ Hz, χ' (dot-dashed), χ'' (solid). The frequencies were chosen such that $\omega_1 < \tau^{-1}$ for the both of the peaks in Fig. 7, hence the notches in χ'', while $\omega_2 > \tau^{-1}$ for all H_z.
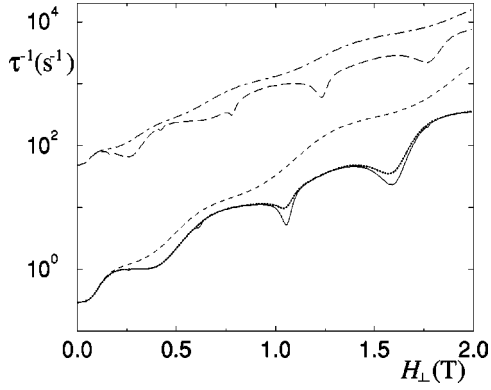
FIG. 10. Oscillations in the relaxation rate as a function of $H_\perp$. The lower and upper groups of curves correspond to H_z $=0.0002$ T, $k_B T=3.0$ K and $H_z=0.01$ T, $k_B T=5.0$ K, respectively. The individual curves correspond to different angles ϕ: 0° (dashed and dot-dashed), 43° (dotted), and 45° (solid and long dashed).

FIG. 12. Log-log scale schematic of Lorentzian curves on top of each other similar to the $H_z \approx 0$ T situation for Mn$_{12}$. The higher the curves are the narrower they get and, on the other hand, the higher the H_z the lower the observed resonances are. The relaxation rate is determined by the fastest possible rate, depicted in the figure with the thick solid line.

hand side of the peak in Im[$\chi(H_z;\omega)$]. For lower ω, $\omega\tau$ can cross the maximum point and the picture with the peaks and valleys turns upside down. These points are illustrated in Fig. 9 for a case corresponding to one of the curves in Fig. 7.

Let us next consider a different scheme, keeping H_z and ϕ fixed and varying $H_\perp$ starting from zero field. The case $H_z \approx 0$ T is of particular interest because it allows comparison to recent experiments by Wernsdorfer done on the related material Fe$_8$, cf. Ref. 50—the experimental data showed clear oscillations of the relaxation rates as a function of $H_\perp$ in the thermally activated regime. By choosing parameters in the feasible range of these experiments, we find somewhat similar oscillations also for Mn$_{12}$. Figure 10 shows first the relaxation rates for two different combinations of temperature and the longitudinal field: $T=3.0$ K and $H_z=0.2$ mT to show the behavior close to (or at) the peak maximum and at a lower temperature, and $T=5.0$ K and $H_z=10$ mT as an example of the behavior further away from the maximum and at a higher temperature. Also the ϕ dependence is shown.

For $\phi=0°$, the gentle oscillations resembling a strongly-smeared staircase stem from the fact that the lower (in terms of energy; higher in terms of rates) resonances are broadened
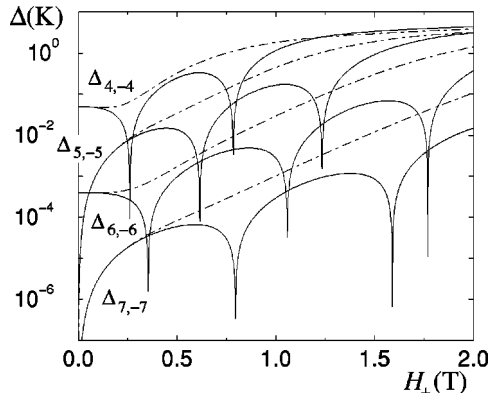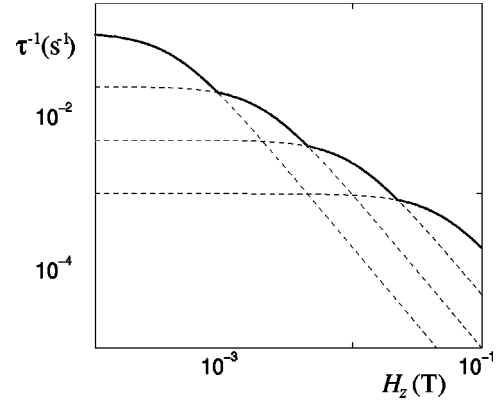
and one by one start to dominate the relaxation, see the dot-dashed curves in Fig. 11 for the tunnel splittings and Fig. 12 for the general idea. All the additional structure, seen for ϕ $=45°$, is due to the oscillations in the tunnel splittings and the suppression of some of the resonances. The positions of the notches can be compared with the structure of $\Delta_{m,-m}$ in Fig. 11 and one finds that for smaller H_z the relaxation takes place via the lower-lying resonances such as $m=\pm 6$ and $m=\pm 7$; further away from the maximum, the broader resonances between states $m=\pm 4$ and $m=\pm 5$ act as the dominant relaxation paths.

Figures 13 and 14 show the real part of the susceptibility χ' corresponding to the two cases of Fig. 10. The purpose of the different frequencies is to show that also here one can choose the structure of interest and study it by tuning the frequency to fulfill $\omega\tau \approx 1$. In both figures, there are regimes where the susceptibility can be varied by a factor of 5; in Ref. 50 the oscillations were quite clear already with the amplitude being a mere 20% of the signal.
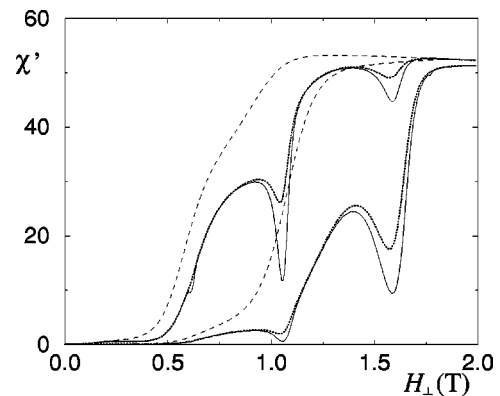

FIG. 11. Tunnel splittings $\Delta_{m,-m}$ for four resonances relevant for Fig. 10. The dot-dashed and solid lines denote the angles ϕ $=0°$ and 45°, respectively.

FIG. 13. Real part of the susceptibility for $H_z=0.2$ mT, $k_B T$ $=3.0$ K, and for the angles $\phi=0°$ (dashed), 43° (dotted), and 45° (solid). The upper three curves correspond to the frequency ω $=10$ Hz and the lower ones to $\omega=50$ Hz. The line types correspond to those for τ^{-1} in Fig. 10.
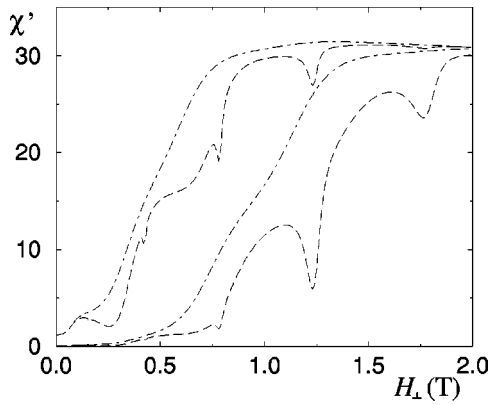
FIG. 14. Real part of the susceptibility for $H_z = 10$ mT, $k_B T = 5.0$ K, and for the angles $\phi = 0°$ (dot-dashed) and $45°$ (long dashed), i.e., the line types correspond to those in Fig. 10. The upper pair of curves corresponds to $\omega = 250$ Hz and the lower one to $\omega = 1250$ Hz.

C. Discussion—relevance to experiments

So far we have considered the simple model comprising a single spin coupled to a phonon bath but, as was pointed out in the introduction, in real samples there are also other kinds of interactions. In this section, we consider the additional features arising from the hyperfine and/or dipolar interactions and aim to point out the experimentally relevant aspects of the results obtained above.

Let us first recall some experimental facts concerning relaxation measurements and results—these underlie also the understanding and appreciation of the susceptibility measurements. Relaxation rates are typically measured by first magnetizing the sample to saturation, and then reversing the direction of the field and measuring the resulting magnetization as a function of time. The initial relaxation is observed to be nonexponential—this is attributed to dipolar interactions, see below—while, at later times, it becomes exponential.[15] Several authors have proposed an extended exponential $M(t) = M(0)\exp[-(t/\tau)^\beta]$ to account for both of these regimes with just one additional fitting parameter β. In Ref. 15 it was found that β varies from $\beta \approx 0.5$ below 2.0 K to $\beta \approx 1$—usual exponential relaxation—roughly above 2.4 K. The thus obtained relaxation rates exhibit a series of broad Lorentzian-shaped resonances; their height and location correspond to tunneling-assisted relaxation three to four levels below the top of the barrier.

This shows two clear differences as compared to the present work: in experiment, the relaxation may be nonexponential even though the single-spin model always yields exponential behavior, and no satellite peaks are observed (see Ref. 27 for exceptions). In order to understand these discrepancies, let us first consider the effect of the nuclei via the hyperfine interactions and then the intermolecular dipolar interactions.

Hyperfine interactions. In Mn_{12}, all the manganese nuclei have magnetic momenta and the hyperfine interaction between the nuclei and the molecular spin state is relatively large, of the order of 10 mT. Recently, several authors have investigated how this affects tunneling and the relaxation in Mn_{12}.[12,14,19,20,22] For the present purposes, the relevant effect of the hyperfine interactions is to induce an *intrinsic* Gauss-

ian broadening, of the width $\sigma_{hyp} \approx 6$ mT,[35] to all levels, i.e., the nuclear spins are importantly dynamic and their influence on the molecular spin cannot be reduced to a rigid but spatially varying background field. Simultaneously with the broadening, the hyperfine interactions reduce the tunneling amplitudes of the resonances for which $\Delta < \sigma_{hyp}$—this should lead to reduced peak heights in $\tau^{-1}(H_z)$.

With this in mind, let us consider the different regimes in terms of the relative magnitudes of the tunnel splitting and the hyperfine broadening. First, for resonances with $\Delta \gg \sigma_{hyp}$ the shapes of the resonances are expected to be Lorentzian with the widths determined by the tunnel splittings Δ. This is the regime, where all our results apply. In the other extreme, $\Delta \ll \sigma_{hyp}$, the resonances should be essentially suppressed providing one possible explanation why the sharp satellite peaks are not observed in experiments.[52] Note that the minuscule phonon-induced broadening or dephasing is hidden under the hyperfine broadening and cannot be seen. In this regime, one could in principle try and extend the present theory by adding by hand a strong dephasing term to the nondiagonal density matrix elements. The intermediate regime where $\Delta \approx \sigma_{hyp}$ is the most interesting of the three cases. In this regime, the peak shape should be a combination of Lorentzian and Gaussian curves and, depending on which one of Δ or σ_{hyp} is larger, one of the shapes should dominate. In the tail region, i.e., away from the peak maxima, the Lorentzian tails dominate and it has been suggested that this together with experimental error bars may obscure the resolution between the two types of curves, cf., e.g., Ref. 22.

The immediate conclusion from these considerations is that, if the application of $H_\perp$ broadens some of the tunnel splittings $\Delta_{m,m'}$ to exceed σ_{hyp}, the corresponding resonance should become observable. If, on the other hand, the transverse field is applied along one of the hard axes, a given resonance becomes suppressed for certain special values of $H_\perp$; in the presence of the hyperfine interactions this should happen already when $\Delta_{m,m'}$ becomes smaller than σ_{hyp}. The intermediate regime can be intentionally achieved by tuning the tunnel splitting from being well below σ_{hyp} to above it. This may provide means to probe the Gaussian broadening, see also the subsection below focusing on the advantages of susceptibility measurements.

Dipolar interactions. The intermolecular spin-spin interactions are of dipolar form and they are weaker in Mn_{12} than, e.g., in Fe_8. Due to their short range, the dipolar fields can vary in space changing the local field at the position of the individual molecules. In our view, the essential difference between the hyperfine and dipolar interactions can be stated as follows: even if one could measure the response of a single molecule, this would always be dressed by the level broadening and reduction in tunneling amplitudes due to hyperfine interactions intrinsic to each molecule; the dipolar fields, on the other hand, just change the molecule's local electromagnetic environment.

In experiment, the relaxation of the magnetization $M(t)$ leads to time-dependent dipolar fields and, in order to describe the relaxation correctly, it would be necessary to solve for $M(t)$ self-consistently, for simulations see, e.g., Refs. 19 and 53. However, it is this time-dependent field that provides an explanation to the initial nonexponential relaxation. For

example in Ref. 15, it is therefore concluded that the deviation from a single-exponential relaxation, i.e., $\beta \neq 1$, demonstrates the important role of the dipolar interactions and dynamics of the spin distribution. It should be kept in mind, though, that also a static distribution of local fields (be it dipolar or not)—and hence relaxation rates $\tau^{-1}(H_z^{\text{local}})$—leads to a superposition of exponential rates, which looks nonexponential. Such a distribution of fields also hides all features in $\tau^{-1}(H_z)$ that are sharper than this distribution.

The time dependence of the dipolar fields owes to the fact that the sample is first magnetized and, as the field direction is abruptly reversed, the dipolar distribution finds itself far from equilibrium and quickly starts to relax. The reason for such experiments is the strong response from almost all the spins.

In anticipation of the discussion on susceptibility, let us consider the dipolar distributions at equilibrium. By distribution we mean spatial variations in the dipolar field at the locations of the individual molecules. First, for $H_z \approx 0$ T, the annealed (not quenched) distribution is random but due to the low temperatures, $k_B T \ll E_{\pm 9} - E_{\pm 10}$, almost all the spins are aligned with the easy z axis—randomly pointing to the positive and negative directions—and only contribute to the local longitudinal field. On the other hand, the equilibrium magnetization is close to saturation already for $H_z \approx H_1$, thus drastically narrowing the dipolar distribution—e.g., for $T = 3.0$ K (5.0 K) and $H_z = H_1$, more than 95% (85%) of all the spins are aligned parallel to H_z and all the molecules feel essentially the same field. Such distributions have been experimentally verified in Fe$_8$, cf. Ref. 51.

Susceptibility. The influence of the dipolar dynamics on relaxation can be avoided almost completely by measuring linear response to a small ac field, i.e., the ac susceptibility, instead of $M(t)$. This has the advantage that the system is probed in its equilibrium state and ideally by a small enough field that in itself does not perturb the equilibrium. Therefore we propose that the susceptibility measurements provide a gentle or noninvasive means to probe the relaxation dynamics in absence of the time-dependent dipolar distribution. Furthermore, while the hyperfine interactions cannot be tuned, the static distribution can be made markedly narrower by a finite H_z, see above. As, on the other hand, χ_0 decreases with increasing H_z, the first group of resonances, close to H_1, is especially attractive for investigating the oscillations in the relaxation rates as well as the hyperfine fields themselves. All of the resonances around H_1 depend strongly on $H_\perp$ and can be broadened such that $\Delta > \sigma_{\text{hyp}}$ making them observable; the peaks can also be selectively suppressed if $\phi \approx 45°$. The hyperfine fields may even simplify the observation of the suppressions as very narrow peaks are strongly reduced in height. For a sharp dipolar distribution, we expect that also the crossover between Lorentzian and Gaussian shapes of $\tau^{-1}(H_z)$ should be observable when changing the tunnel splittings with the transverse field.

V. CONCLUSIONS

To conclude, we present a diagrammatic description of the spin dynamics of the molecular magnet Mn$_{12}$. The work

focuses on the regime of thermally activated tunneling, i.e., $T > 2.0$ K, and emphasizes the phenomena that could be observed for strong transverse magnetic fields. In the calculations, we study the dynamics of a single spin $S = 10$ coupled to a phonon bath. The role of the phonons is in the thermal activation of the spins to states with higher energies and larger tunneling amplitudes.

As the first main result, we calculate the dynamic susceptibility $\chi(\omega)$ starting from the same microscopic Hamiltonian as is used for the relaxation rates. Susceptibility is found to reflect the rich structure found in $\tau^{-1}(H_z)$ and we argue that susceptibility measurements are in fact more sensitive and better controlled in terms of time scales and also the dipolar interactions than the relaxation experiments.

All the results obtained are calculated using the eigenbasis of the spin Hamiltonian, which naturally accounts for strong transverse magnetic fields. A strong transverse magnetic field enhances tunneling through the anisotropy barrier and enables relaxation via eigenstates further away from the top of the barrier. In relaxation or susceptibility measurements, this would lead to shifted and higher resonances. The tunnel splittings are found to be very sensitive to the azimuth angle ϕ of the transverse field $H_\perp$. It is found that, in the directions $\phi = \pi(2n+1)/4$, the tunnel splittings exhibit alternating minima and maxima and become totally suppressed at certain values of $H_\perp$. This phenomenon is attributed to the interference of the geometrical or Berry phase of alternative tunneling paths, with a destructive interference leading to the suppressions. As the second major result, we predict that these oscillations in the tunnel splittings should be observable both in the relaxation rates and the susceptibility.

APPENDIX A: SPIN-PHONON RATES

In this appendix, we give the phonon-induced transition rates Σ between different spin states—the details can be found elsewhere.[38] In the d basis, the elements $\Sigma_{dd_1, d'd_1'}(t - t')$ correspond to transitions between the elements $\rho_{d'd_1'}$ and ρ_{dd_1} of the reduced density matrix. The two times t and t' ($t' < t$; below $\tau \equiv t - t'$) define the interval over which the interaction takes place. Let us first write down the full time-dependent result,

$$\Sigma(\tau)_{dd_1, d'd_1'} = \sum_{m_1, \dots, m_4} G_{m_2 m_1, m_3 m_4} \cdot \left\{ \langle m_1 | d' \rangle \langle d | m_2 \rangle \right.$$

$$\times \langle m_3 | d_1 \rangle \langle d_1' | m_4 \rangle [e^{-i(E_d - E_{d_1'})(\tau)} \Gamma(-\tau)$$

$$\left. + e^{-i(E_d' - E_{d_1})(\tau)} \Gamma(\tau)]\right.$$

$$-\sum_{\bar{d}} \langle \bar{d}|m_2\rangle\langle m_3|\bar{d}\rangle [\delta_{d_1,d_1'}\langle m_1|d'\rangle\langle d|m_4\rangle$$

$$\times e^{-i(E_{\bar{d}}-E_{d_1'})(\tau)}\Gamma(-\tau) + \delta_{d,d'}\langle m_1|d_1\rangle$$

$$\times\langle d_1'|m_4\rangle e^{-i(E_d'-E_{\bar{d}})(\tau)}\Gamma(\tau)]\bigg\}. \quad (A1)$$

The term

$$G_{m_2m_1,m_3m_4} = \sqrt{S_{m_2,m_1}S_{m_3,m_4}}\cdot C_{\xi,\xi'} \quad (A2)$$

($\xi\equiv m_2-m_1, \xi'\equiv m_3-m_4$; for the spin-phonon Hamiltonian considered here, these can take values ± 1 or ± 2) further consists of

$$C_{\xi,\xi'} = \begin{cases} 0, & \text{for } |\xi|\neq|\xi'| \\ 1, & \xi=\xi'=\pm 1 \\ \frac{15}{16}+\frac{1}{8}\delta_{\xi,\xi'}, & |\xi|=|\xi'|=2, \end{cases} \quad (A3)$$

which implies the selection rules arising from the spin-phonon Hamiltonian, and

$$S_{m_2,m_1} = (2m_1+\xi)\sqrt{S(S+1)-m_1(m_1+\xi)} \quad (A4)$$

for $\xi=\pm 1$ or

$$S_{m_2,m_1} = \{[S(S+1)-m_1(m_1+\nu)]$$

$$\times[S(S+1)-(m_1+\nu)(m_1+2\nu)]\}^{1/2} \quad (A5)$$

for $\xi=\pm 2$, $\nu=\text{sgn}(\xi)$. The function $\Gamma(t)$ entering Eq. (A1) contains all the information concerning the phonon spectrum, energies, and temperature,

$$\Gamma(t) = \int_{-\infty}^{\infty} d\omega\,\Gamma(\omega)e^{i\omega t} \quad (A6)$$

$$\equiv \int_{-\infty}^{\infty} d\omega\frac{A^2}{12\rho c^5\hbar^4}\cdot\frac{\omega^3}{e^{\beta\omega}-1}\cdot e^{i\omega t} \quad (A7)$$

$$= \frac{A^2}{12\rho c^5\hbar^4}\cdot\left\{-2\left(\frac{\pi}{\beta}\right)^4\left[\frac{1+2\text{ch}^2\left(\frac{\pi t}{\beta}\right)}{\text{sh}^4\left(\frac{\pi t}{\beta}\right)}\right]\right.$$

$$\left.+i\pi\delta'''(t)\right\}. \quad (A8)$$

This part is defined such that it is independent of the spin states and only contains the term A^2 from the coupling constants that turns out to be constant for all the rates.

The actual transition rates are obtained from Eq. (A1) by integrating over the time difference $\tau=t-t'$. This takes us to the energy representation, combining the exponential factor in Eq. (A1) with the $e^{i\omega(t-t')}$ of the Fourier transform in Eq. (A7). The integration over τ yields

$$\Sigma_{dd_1,d'd_1'} = i\sum_{m_1,\ldots,m_4} G_{m_2m_1,m_3m_4}\cdot\bigg\{\langle m_1|d'\rangle\langle d|m_2\rangle\langle m_3|d_1\rangle$$

$$\times\langle d_1'|m_4\rangle\int_{-\infty}^{\infty}d\omega\left[\frac{\Gamma(\omega)}{-\omega+E_{d'}-E_{d_1}+i\eta}\right.$$

$$\left.+\frac{\Gamma(\omega)}{\omega-E_{d_1'}+E_d+i\eta}\right]-\sum_{\bar{d}}\langle\bar{d}|m_2\rangle$$

$$\times\langle m_3|\bar{d}\rangle\cdot\left[\delta_{d_1,d_1'}\langle m_1|d'\rangle\right.$$

$$\times\langle d|m_4\rangle\int_{-\infty}^{\infty}d\omega\frac{\Gamma(\omega)}{\omega-E_{d_1'}+E_{\bar{d}}+i\eta}$$

$$+\delta_{d,d'}\langle m_1|d_1\rangle$$

$$\left.\left.\times\langle d_1'|m_4\rangle\int_{-\infty}^{\infty}d\omega\frac{\Gamma(\omega)}{-\omega+E_{d'}-E_{\bar{d}}+i\eta}\right]\right\}. \quad (A9)$$

The above integrals are explicitly evaluated in Ref. 38. For the rates between the diagonal states, $d=d_1$ and $d'=d_1'$, the above expressions are greatly simplified. In this case, rates similar to those in, e.g., Ref. 18 are obtained.

With all the contributions to Σ written down, we can find an estimate for the order of magnitude of the elements (the individual rates) $\Sigma_{dd_1,d'd_1'}$. The most interesting piece of information for each state is the *largest rate* coupling that state to other states—this rate plays a key role in justifying the neglect of the nondiagonal states in $\rho(t)$, see Appendix B, as well as in the suppression of the narrow resonances found in the text.

The prefactor in $\Gamma(\omega)$, cf. Eq. (A7), amounts to $7.0\times 10^5 c^{-5}$ s^5 m^{-5} K^{-2}, where the sound velocity c is expressed in meters per second. The units are chosen such that, when ω is expressed in kelvin, also $\Gamma(\omega)$ is given in kelvin. For $\omega>0$ (and also $\omega>k_BT$), i.e., for transitions related with phonon absorption, the energy-dependent part of $\Gamma(\omega)$ strongly decreases for increasing ω; for $\omega<0$, corresponding to phonon emission, $\Gamma(\omega)$ approaches the temperature-independent power-law dependence ω^3. The largest $\Gamma(\omega)$'s are attained for these latter processes in connection with low-energy spin states. The contribution from the spin operators, cf. Eqs. (A4) and (A5), on the other hand, is larger for spin states closest to the top of the barrier and tends to balance the changes in $\Gamma(\omega)$ and reduce the variations in $\Sigma_{dd_1,d'd_1'}$ for different states and for varying H_z. The typical energy scale arising from the spin-phonon rates is found to be $10^{-5}-10^{-4}$ K.

APPENDIX B: CHOICE OF BASIS

In Sec. III, we decidedly formulated the more general equations independent of the chosen basis for $\mathcal{H}_S$. In this appendix, we consider the eigenbases of $\mathcal{H}_S$ or the d basis, in more detail.

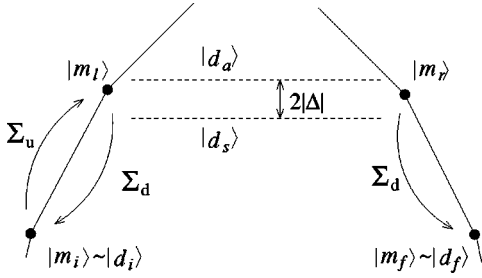The (strong) tunneling poses a problem for the diagram-

FIG. 15. Schematic of the situation discussed in the text. If the spin-phonon coupling denoted by the arrows and Σ's is much weaker than the tunnel coupling Δ between the states $|m_l\rangle$ and $|m_r\rangle$, these states can be thought of as an effective two-state system. The eigenstates of the two-state system are depicted as dashed lines separated in energy by $2|\Delta|$. The subscripts of the Σ's correspond to those used in the text.

matic formulation in the m basis, but this can be easily solved by first diagonalizing $\mathcal{H}_S$ and then expressing all the equations in its eigenbasis. In this d basis, the kinetic equation for the diagonal and off-diagonal density matrix elements reads

$$\dot{\rho}(t)_{d,d}=\sum_{d_1,d_1'}\Sigma_{dd,d_1d_1'}\rho(t)_{d_1,d_1'} \qquad \text{(B1)}$$

and

$$\dot{\rho}(t)_{d,d'}=-i(E_d-E_{d'})\rho(t)_{d,d'}+\sum_{d_1,d_1'}\Sigma_{dd',d_1d_1'}\rho(t)_{d_1,d_1'}, \qquad \text{(B2)}$$

respectively. From the knowledge of (the full) $\rho(t)$ we can again obtain, e.g., the magnetization

$$M(t)=g\mu_B\sum_{d,d'}\sum_m\langle d'|m\rangle m\langle m|d\rangle\rho_{d,d'}(t) \qquad \text{(B3)}$$

$$\equiv g\mu_B\sum_{d,d'}m_{d,d'}\rho_{d,d'}(t), \qquad \text{(B4)}$$

where $m_{d,d'}$ is defined in this way as the matrix element of S_z in the d basis.

When the tunneling rates dominate the kinetic equations, the main features of the eigenstates can be understood in even simpler terms as follows. When a given state is off resonant, there is essentially a one-to-one correspondence between each of the m and d states, i.e., also the d states are localized on one or the other side of the barrier. Close to a resonance, two states m_l and m_r on different sides of the barrier, see Fig. 15, get coupled and form an approximate two-state system described by

$$\mathcal{H}_2=\begin{pmatrix} E_{m_l} & \Delta \\ \Delta^* & E_{m_r} \end{pmatrix}. \qquad \text{(B5)}$$

The nondiagonal elements denote the tunnel splitting as obtained from the diagonalization of the full spin Hamiltonian; the subscripts stand for the left and right sides of the barrier. The eigensolutions to this are the symmetric and antisymmetric combinations of the respective m states

$$|d_s\rangle=\alpha|m_l\rangle+\beta|m_r\rangle, \qquad \text{(B6)}$$

$$|d_a\rangle=\beta|m_l\rangle-\alpha|m_r\rangle \qquad \text{(B7)}$$

that extend through the barrier, see Fig. 15. The factors α and β are the normalized constants

$$\alpha=\frac{\Delta}{\sqrt{\hat{\varepsilon}^2+|\Delta|^2}}, \qquad \text{(B8)}$$

$$\beta=\frac{\hat{\varepsilon}}{\sqrt{\hat{\varepsilon}^2+|\Delta|^2}} \qquad \text{(B9)}$$

with $\hat{\varepsilon}=\frac{1}{2}[(E_l-E_r)-\sqrt{(E_l-E_r)^2+4|\Delta|^2}]$.

The biggest simplification is attained when we argue that, for the most values of H_z, we can restrict our considerations to the diagonal elements of the density matrix. A naive justification for this concerns the stationary values of the density matrix elements [obtained by requiring $\dot{\rho}(t)_{d,d'}=0$]. This leads to the immediate conclusion that all the off-diagonal elements between nonresonant states are negligibly small. Furthermore, the nondiagonal elements are also very small for any pair of resonant states as long as the tunnel splitting of that particular resonance is larger than the spin-phonon rates coupling these states to others, see the end of Appendix A.

We also investigated the temporal behavior of the off-diagonal elements in terms of the reduced model shown in Fig. 15 and the results lend support to the above conclusions. The idea of this simulation was to prepare the system into the state d_i at the initial time t_0, let the system then evolve in time according to the kinetic equation, and see how the off-diagonal elements $\rho(t)_{d_s,d_a}$ and $\rho(t)_{d_a,d_s}$ behave. The resonant pair of states in the figure is similar to the one in Eqs. (B6) and (B7) and it is coupled to two lower, nonresonant states d_i and d_f. The rates depicted in the figure are $\Sigma_u=\Sigma_{ll,ii}$ and $\Sigma_d\approx(\Sigma_{ii,ll}+\Sigma_{ff,rr})/2$. The magnitudes of these rates—as compared to the tunnel splitting $|2\Delta|$—determine two regimes. If $2|\Delta|\gg\Sigma_d$, the amplitudes of the nondiagonal elements are found to quickly reach their maxima $\propto\Sigma_u/|2\Delta|$ and their values orbit around and ''decay'' towards the respective complex stationary values. On the other hand, according to the detailed-balance relation, the stationary values of the diagonal elements are proportional to Σ_u/Σ_d. Hence $\rho(t)_{d,d'}/\rho(t)_{d^{(')}}\propto\Sigma_d/|2\Delta|$ and we can neglect the nondiagonal elements, if $\Sigma_d\ll2|\Delta|$. In this case the kinetic equation, Eqs. (B1) and (B2), becomes very simple: Eq. (B2) can be neglected and the rate Σ acquires the form, cf. Appendix A,

$$\Sigma_{d'd',dd}=\pm G_{dd',d'd}\frac{\pi A^2}{12\rho c^5\hbar^4}\cdot\frac{\Delta E^3}{e^{\beta\Delta E}-1}, \qquad \text{(B10)}$$

where

$$G_{dd',d'd}=\sum_{m_1,m_2}\sum_{m_3,m_4}G_{m_4m_3,m_2m_1}\cdot\langle d'|m_4\rangle\langle m_3|d\rangle\langle d|m_2\rangle$$
$$\times\langle m_1|d'\rangle \qquad \text{(B11)}$$

contains all the details of the spin-phonon coupling, see Appendix A. In the opposite case, $2|\Delta|\ll\Sigma_d$, the nondiagonal

elements do not perform orbiting motion in the complex plane but increase monotonously to roughly one half of $\rho_{d(')}^{(0)}$. In this case, the off-diagonal elements clearly cannot be neglected.

For Mn_{12} we can attain the whole range of cases: for the most strongly coupled level(s) $2|\Delta| \gg \Sigma_d$, while for the lower levels, $2|\Delta| \ll \Sigma_d$. In the former case, the diagonal elements $\rho_d(t)$ are sufficient in describing the system whereas, in the latter case, we either have to include the nondiagonal states or restrict our considerations to magnetic fields for which $\Delta E \gg \Sigma_d$ for all the levels, cf. Ref. 16. In the text, we neglect the nondiagonal elements in the calculation of $\chi(\omega)$ and in some of the analytical considerations but compare the two cases in Sec. IV.

APPENDIX C: LAPLACE TRANSFORMATION

In this appendix, we consider the Laplace transformation

$$f(z) \equiv \int_0^\infty dt\, e^{-izt} f(t) \tag{C1}$$

of the kinetic equation, Eq. (10). We also give another proof of the applicability of the Markov approximation in calculating the relaxation rates.

The kinetic equation is readily transformed into

$$-iz\rho(z) - \rho(t=0) = -iL_0\rho(z) + \Sigma(z)\rho(z) \tag{C2}$$

$$\Rightarrow \rho(z) = \frac{\rho(t=0)}{-iz + iL_0 - \Sigma(z)}. \tag{C3}$$

The poles of Eq. (C3), i.e., the solutions of $-iz_i + iL_0 - \Sigma(z_i) = 0$, yield the exact eigenvalues to the kinetic equation: $z_i = \omega_i + i/\tau_i$. For the slowest mode of the time evolution, one can consider the expansion

$$\Sigma(z_1) \approx \Sigma(0) + z_1 \cdot \left. \frac{\partial\Sigma(z)}{\partial z} \right|_{z=0} + \cdots. \tag{C4}$$

The prefactor of the z_1 may be evaluated to be proportional to $[\tau_1 \cdot \min\{\Delta E, k_B T, D\}]^{-1}$, i.e., to the maximal ratio between the interwell relaxation rate $1/\tau_1$ and the other characteristic energy scales in the problem: level spacing and/or splitting ΔE, temperature $k_B T$, and the cutoff of the phonon spectrum D [in Ref. 38, a cutoff D is introduced in order to assure that all the integrals arising from Eq. (A9) are convergent]. It turns out that the actual relaxation rates are several orders of magnitude smaller than any other energy scale and it becomes safe to approximate

$$\rho(z) \approx \frac{\rho(t=0)}{-iz + iL_0 - \Sigma(0)} = \frac{\rho(t=0)}{-iz - W}, \tag{C5}$$

where $\Sigma(0)$ has been identified as the constant Σ of the Markov approximation above and W is defined accordingly, cf. Eq. (11). This approximation is valid for the relaxation mode and time τ_1,

$$\rho^{(1)}(z) = \frac{\rho^{(1)}(t=0)}{-iz - 1/\tau_1}, \tag{C6}$$

but the Markov approximation may give erroneous results for the faster eigenmodes for which Eq. (C5) no longer holds true.

APPENDIX D: LORENTZIAN PEAK SHAPES

The series of peaks found in the relaxation rates/times, cf. Fig. 4, may be understood in terms of different relaxation paths, each path with a possible tunneling channel giving rise to a peak—see Ref. 18 for nice illustrations of the paths. In this appendix, we sketch a derivation that aims to show that the Lorentzian peak shapes are actually something to be expected.

When the spin system is somehow disturbed away from equilibrium and then let relax, it quickly acquires a metastable state, a thermal equilibrium separately on each side of the barrier. This initial thermalization into the metastable state is driven by the spin-phonon interaction that can change the spin states m by ± 1 or ± 2. At a much longer time scale, the system relaxes over the barrier towards the real equilibrium configuration. For the relaxation to take place, the crucial step is the final transition that transfers the spin onto the other side of the barrier. We can distinguish two regimes in terms of how this critical transition takes place. In absence of tunneling, e.g., in off-resonance conditions, the relaxation is only possible over the top of the barrier, while for relatively strong tunnel splitting and for resonant conditions, the dominant path is via tunneling across the barrier well below its top. When the tunneling is weak compared with the spin-phonon interaction, the tunneling rate is the bottle neck for the relaxation to take place. In Mn_{12}, this is the case for tunneling between the low-lying states with $|m| > 4$ (for $H_z \approx 0$ T). However, for the experimentally relevant resonances, the tunneling is strong and takes place between the higher states. In this case, the spin actually oscillates back and forth through the barrier until it relaxes to some lower state on either side of the barrier. This is the case of interest here.

In the strong-tunneling regime, the system is best described in terms of the d basis where it suffices to consider the diagonal elements of the density matrix. In order to get a more intuitive picture of the relaxation, let us consider a situation where the system has been prepared onto one side of the barrier and has reached the metastable thermal equilibrium there. This initial condition is convenient for two purposes: first, the relaxation only proceeds into one direction and, second, the phonon-induced transitions on this one side of the barrier are accounted for by the thermal probabilities $\tilde{\rho}_d$ (tilde denotes the metastable state and we write just one index for the diagonal matrix elements). Let us further consider relaxation via a single tunneling resonance and take into account the states and transition processes illustrated in Fig. 16. The system starts in the initial state d_i (localized onto the left side of the barrier, $\sim m_i$), is then activated onto resonance into either the symmetric or antisymmetric state, denoted by d_s and d_a, respectively, and at some point is transferred down to the final state d_f (localized onto the right side of the barrier, $\sim m_f$). The subsequent intravalley relaxation is so fast that after the transition to d_f the relaxation can be considered complete. The states d_s and d_a extend through the barrier and this is the key point of the present
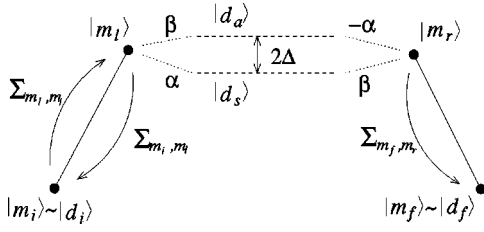
FIG. 16. Illustration of the parameters discussed in the text: states in the m and d bases, transition rates $\Sigma_{m,m'}$, and factors $\pm\alpha$ and β from Eq. (B5).

discussion: the spin is transferred through the barrier in a single step, the rate being determined by thermal activation but also by the magnetic-field dependent amplitudes α and β, from Eqs. (B6) and (B7), for the two extended states to be on either side of the barrier. These amplitudes determine the relative probabilities for the activation process to couple to the resonant states.

The above discussion can be formulated in the language of a master equation:

$$\dot{\widetilde{\rho}}_{d_s}(t)=0$$

$$\approx \Sigma_{d_s,d_i}\widetilde{\rho}_{d_i}(t)-(\Sigma_{d_f,d_s}+\Sigma_{d_i,d_s})\widetilde{\rho}_{d_s}(t)$$

$$\approx|\langle d_s|m_l\rangle|^2\Sigma_{m_l,m_i}\widetilde{\rho}_{d_i}(t)$$

$$-(|\langle d_s|m_r\rangle|^2\Sigma_{m_f,m_r}+|\langle d_s|m_l\rangle|^2\Sigma_{m_i,m_l})\widetilde{\rho}_{d_s}(t)$$

$$=|\alpha|^2\Sigma_{m_l,m_i}\widetilde{\rho}_{d_i}(t)$$

$$-(|\beta|^2\Sigma_{m_f,m_r}+|\alpha|^2\Sigma_{m_i,m_l})\widetilde{\rho}_{d_s}(t) \tag{D1}$$

$$\dot{\widetilde{\rho}}_{d_a}(t)=0$$

$$\approx \Sigma_{d_a,d_i}\widetilde{\rho}_{d_i}(t)-(\Sigma_{d_f,d_a}+\Sigma_{d_i,d_a})\widetilde{\rho}_{d_a}(t),$$

$$\approx|\langle d_a|m_l\rangle|^2\Sigma_{m_l,m_i}\widetilde{\rho}_{d_i}(t)$$

$$-(|\langle d_a|m_r\rangle|^2\Sigma_{m_f,m_r}+|\langle d_a|m_l\rangle|^2\Sigma_{m_i,m_l})\widetilde{\rho}_{d_a}(t)$$

$$=|\beta|^2\Sigma_{m_l,m_i}\widetilde{\rho}_{d_i}(t)$$

$$-(|\alpha|^2\Sigma_{m_f,m_r}+|\beta|^2\Sigma_{m_i,m_l})\widetilde{\rho}_{d_a}(t). \tag{D2}$$

The approximate equalities are just a reminder that we have neglected, e.g., the contributions from states above the resonance as well as the return possibility from state d_f. These equations can be simplified by the assumption $\Sigma_{m_i,m_l} \approx \Sigma_{m_f,m_r}$ which is reasonable for a pair of resonant

states—as a result, the Σ's can be taken out of the brackets in the last forms of the above formulas. By further noting that due to normalization $|\alpha|^2+|\beta|^2=1$ and that the resulting probabilities are time independent, we obtain

$$\widetilde{\rho}_{d_s}\approx|\alpha|^2\frac{\Sigma_{m_l,m_i}}{\Sigma_{m_i,m_l}}\widetilde{\rho}_{d_i},$$

$$\widetilde{\rho}_{d_a}\approx|\beta|^2\frac{\Sigma_{m_l,m_i}}{\Sigma_{m_i,m_l}}\widetilde{\rho}_{d_i}.$$

The ratio of the Σ's is just the thermal factor $\exp[-\beta(E_l-E_i)]$, cf. detailed balance, and $\widetilde{\rho}_{d_i}$ is the thermal probability to be in a state with energy E_i over the lowest energy E_{-10} on the left-hand side (for $H_z>0$). Together these yield a factor $c\cdot\exp[-\beta(E_l-E_{-10})]$, where c is a normalization constant equal to $\widetilde{\rho}_{-10}$ which is close to unity for the temperatures of interest.

In the next and final step, the relaxation rate is obtained from the knowledge of these probabilities and the rates to be dragged down on the right-hand side of the barrier, i.e.,

$$\tau^{-1}\approx \Sigma_{d_f,d_s}\cdot\widetilde{\rho}_{d_s}+\Sigma_{d_f,d_a}\cdot\widetilde{\rho}_{d_a}$$

$$\approx|\beta|^2\Sigma_{m_f,m_r}\widetilde{\rho}_{d_s}+|\alpha|^2\Sigma_{m_f,m_r}\widetilde{\rho}_{d_a}$$

$$\approx 2|\alpha|^2|\beta|^2\Sigma_{m_f,m_r}c\cdot e^{-\beta(E_i-E_{-10})}. \tag{D3}$$

The exponential factor is just the effective Arrhenius factor seen in experiments, $\frac{1}{2}c\Sigma_{m_f,m_r}=\tau_0^{-1}$, and

$$4|\alpha|^2|\beta|^2=\frac{(2|\Delta|)^2}{(E_{m_l}-E_{m_r})^2+(2|\Delta|)^2}. \tag{D4}$$

Here $2|\Delta|$ is the tunnel splitting. It is more or less independent of H_z but $\xi\equiv E_{m_l}-E_{m_r}$ can be tuned with the magnetic field. In terms of the field, the width of the resonant peak at its half maximum is

$$\delta H_z=\frac{4|\Delta|}{g\mu_B|m_l-m_r|}. \tag{D5}$$

This sketch of a derivation introduces all the factors seen in experiments: the Arrhenius law with a reasonable prefactor τ_0^{-1}, that depends weakly on temperature and the particular resonance, see the two last paragraphs of Appendix A, and peaks of accelerated relaxation superimposed on it. The peak heights or the relaxation rates on resonance are found to correspond to the Boltzmann or Arrhenius factor with the energy corresponding to the effective barrier height. The peak shape is Lorentzian as observed in experiment with widths given by precisely the tunnel splittings.

[1] J.R. Friedman, M.P. Sarachik, J. Tejada, and R. Ziolo, Phys. Rev. Lett. **76**, 3830 (1996).

[2] J.M. Hernandez, X.X. Zhang, F. Luis, J. Bartolome, J. Tejada, and R. Ziolo, Europhys. Lett. **35**, 301 (1996).

[3] L. Thomas, F. Lionti, R. Ballou, D. Gatteschi, R. Sessoli, and B. Barbara, Nature (London) **383**, 145 (1996).

[4] J.M. Hernandez, X.X. Zhang, F. Luis, J. Tejada, J.R. Friedman, M.P. Sarachik, and R. Ziolo, Phys. Rev. B **55**, 5858 (1997).

[5] F. Luis, J. Bartolome, J.F. Fernandez, J. Tejada, J.M. Hernandez, X.X. Zhang, and R. Ziolo, Phys. Rev. B **55**, 11 448 (1997).

[6] A. Ganeschi, D. Gatteschi, and R. Sessoli, J. Am. Chem. Soc. **113**, 5873 (1991); R. Sessoli, D. Gatteschi, A. Caneschi, and M.A. Novak, Nature (London) **365**, 141 (1993).

[7] R. Sessoli, Mol. Cryst. Liq. Cryst. **274**, 145 (1995).

[8] Some authors do report possible observations of dipolar effects, especially at low temperature, see, e.g., Refs. 15 and 35.

[9] The division between thermally activated and tunneling-enhanced relaxation depends on typical experimental time scales. In relaxation measurements, the magnetization first relaxes faster than exponentially and only asymptotically reaches an exponential regime. For $T > 3$ K, almost all the spins relax before reaching this stage. In susceptibility experiments, on the other hand, the relevant time scale is the measurement frequency and this can keep up with the relaxation rate up to 5–6 K.

[10] J. Villain, F. Hartmann-Boutron, R. Sessoli, and A. Rettori, Europhys. Lett. **27**, 159 (1994).

[11] P. Politi, A. Rettori, F. Hartmann-Boutron, and J. Villain, Phys. Rev. Lett. **75**, 537 (1995).

[12] F. Hartman-Boutron, P. Politi, and J. Villain, Int. J. Mod. Phys. B **10**, 2577 (1996).

[13] M.A. Novak and R. Sessoli, in *Quantum Tunneling of Magnetization*, edited by L. Gunther and B. Barbara (Kluwer, Dordrecht, 1995).

[14] D.A. Garanin and E.M. Chudnovsky, Phys. Rev. B **56**, 11 102 (1997).

[15] L. Thomas, A. Caneschi, and B. Barbara, Phys. Rev. Lett. **83**, 2398 (1999).

[16] F. Luis, J. Bartolome, and J.F. Fernandez, Phys. Rev. B **57**, 505 (1998).

[17] A. Fort, A. Rettori, J. Villain, D. Gatteschi, and R. Sessoli, Phys. Rev. Lett. **80**, 612 (1998).

[18] M.N. Leuenberger and D. Loss, Europhys. Lett. **46**, 692 (1999); Phys. Rev. B **61**, 1286 (2000).

[19] N.V. Prokof'ev and P.C.E. Stamp, Phys. Rev. Lett. **80**, 5794 (1998).

[20] D.A. Garanin, E.M. Chudnovsky, and R. Schilling, cond-mat/9911055 (unpublished).

[21] M. Al-Saqer, V. V. Dobrovitski, B. N. Harmon, and M. I. Kastnelson, cond-mat/9909278 (unpublished).

[22] I. Tupitsyn and B. Barbara, cond-mat/0002180 (unpublished).

[23] T. Pohjola and H. Schoeller, Physica B **284-288**, 589 (2000).

[24] E. Chudnovsky and J. Tejada, *Macroscopic Quantum Tunneling of the Magnetic Moment* (Cambridge University Press, Cambridge, 1998), Chap. 6.

[25] The calculation of the time- and frequency-dependent specific heat of Ref. 26 resembles the susceptibility calculation presented in this paper.

[26] J.F. Fernandez, F. Luis, and J. Bartolome, Phys. Rev. Lett. **80**, 5659 (1998); F. Fominaya, J. Villain, T. Fournier, P. Gandit, J. Chaussy, A. Fort, and A. Caneschi, Phys. Rev. B **59**, 519 (1999).

[27] A.D. Kent, Y. Zhong, L. Bokacheva, D. Ruiz, D.N. Hendrickson, and M.P. Sarachik, Europhys. Lett. **49**, 521 (2000); Y. Zhong, M.P. Sarachik, J. Yoo, and D.N. Hendrickson, cond-mat/0006114 (unpublished).

[28] A.L. Barra, D. Gatteschi, and R. Sessoli, Phys. Rev. B **56**, 8192 (1997).

[29] Y. Zhong, M.P. Sarachik, J.R. Friedman, R.A. Robinson, T.M. Kelley, H. Nakotte, A.C. Christianson, F. Trouw, S.M.J. Aubin, and D.N. Hendrickson, J. Appl. Phys. **85**, 5636 (1999).

[30] R. Sessoli, H.L. Tsai, A.R. Shake, S. Wang, J.B. Vincent, K. Folting, D. Gatteschi, G. Christou, and D.N. Hendrickson, J. Am. Chem. Soc. **115**, 1804 (1993).

[31] This bears analogy to the related molecular magnet Fe$_8$, which has hard, medium, and easy axes—the interference effects in the tunnel splittings appear when the external magnetic field is oriented parallel to the hard axis.

[32] Similar results were recently reported in Ref. 22; see Ref. 33 for a detailed analysis of the interference effects.

[33] M.N. Leuenberger and D. Loss, cond-mat/0006075 (unpublished).

[34] In Ref. 21 the authors calculate the energy spectrum for Mn$_{12}$ starting from the magnetic momenta of the 12 Mn atoms and find different level splittings to those predicted by the simple $S = 10$ model. The discrepancy varies between different pairs of states and as ratio varies between 0.8 to 5 from higer to lower states, respectively. Such details do not affect the essence of this paper and may be inserted as parameters into the calculation.

[35] W. Wernsdorfer, R. Sessoli, and D. Gatteschi, Europhys. Lett. **47**, 254 (1999).

[36] This choice of parameter values was recently questioned (Ref. 37) but the qualitative results of Sec. IV are robust against changes in the details of the spin-phonon coupling. This is due to: (i) the magnitude of the coupling constants scales the results but this is counterbalanced by the uncertainty in the sound velocity c; (ii) whether the spin state can change in steps of one, two or some larger amount, also mainly affects the scaling of the results; (iii) the coupling is too weak to significantly influence the energies or the tunneling of the spins.

[37] E.M. Chudnovsky and D.A. Garanin, Europhys. Lett. **52**, 245 (2000).

[38] T. Pohjola and H. Schoeller, cond-mat/0005135 (unpublished).

[39] D.A. Garanin, J. Phys. A **24**, L61 (1991).

[40] H. Schoeller and G. Schön, Phys. Rev. B **50**, 18 436 (1994); J. König, J. Schmid, H. Schoeller, and G. Schön, *ibid.* **54**, 16 820 (1996).

[41] Rigorously taken, instead of $\rho(t') \approx \rho(t)$, we should use $\rho(t') = e^{i\mathcal{H}_S(t-t')}\rho(t)e^{-i\mathcal{H}_S(t-t')}$ and insert this into Eq. (10). Combining the exponential factors yields the expressions of Refs. 45 and 18. This procedure complicates the correspondence of the indices in the equations and in the diagrams, and, as this is found to make very little difference to the final results, (Ref. 42) we neglect this step here.

[42] We performed the calculation with both kinds of Markov approximations and the results did not show any significant differences. It is also noteworthy that when using only the diagonal states of the eigenbasis the two approximations become equal.

[43] We have solved the problem numerically for the full density matrix in both bases, i.e., either first diagonalizing the spin part or taking the tunneling matrix elements into account to all orders in the m basis. The results are of course equivalent.

[44] R. Kubo, M. Toda, and N. Hashitsume, *Statistical Physics II, Nonequilibrium Statistical Mechanics* (Springer, New York, 1985).

[45] K. Blum, *Density Matrix Theory and Applications*, 2nd ed. (Plenum Press, New York, 1996), Chap. 8.

[46] G. Belessa, N. Vernier, B. Barbara, and D. Gatteschi, Phys. Rev. Lett. **83**, 416 (1999).

[47] W. Wernsdorfer and R. Sessoli, Science **284**, 133 (1999).

[48] D. Loss, D.P. DiVincenzo, and G. Grinstein, Phys. Rev. Lett. **69**, 3232 (1992); J. von Delft and C.L. Henley, *ibid.* **69**, 3236 (1992).

[49] A. Garg, Europhys. Lett. **22**, 205 (1993).

[50] W. Wernsdorfer, Physica B **284–288**, 1231 (2000); W. Wernsdorfer (private communication).

[51] W. Wernsdorfer, T. Ohm, C. Sangregorio, R. Sessoli, D. Mailly, and C. Paulsen, Phys. Rev. Lett. **82**, 3903 (1999).

[52] For this reason, the features in, e.g., Fig. 11 that depend on $\Delta_{6,-6}$

and $\Delta_{7,-7}$ may be unobservable for transverse fields below 1–1.5 T, but the features do persist to higher fields than what is shown here.

[53] T. Ohm, C. Sangregorio, and C. Paulsen, Eur. Phys. J. B **6**, 195 (1998); J. Low Temp. Phys. **113**, 1141 (1998).